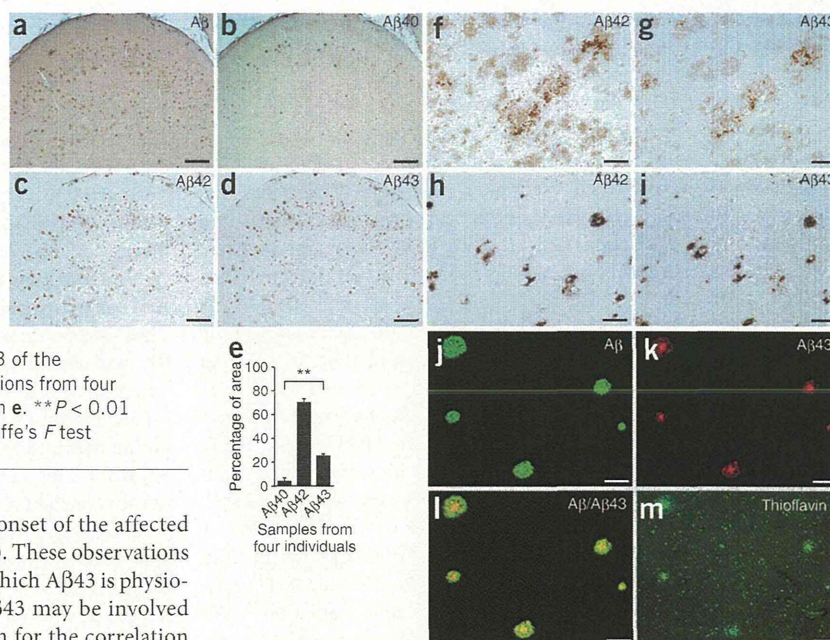

Figure 8 Aβ43 in amyloid plaques in Alzheimer's disease brains. (**a–m**) Serial sections of the hippocampal region (**a–d**,**h**,**i**,**j–m**) and the frontal cortical region of brains from individuals with Alzheimer's disease (**f**,**g**) were stained with 4G8 (total Aβ), C40 (Aβ1–40), C42 (Aβ1–42) and C43 (Aβ1–43), as well as thioflavin S, as indicated. The single staining (**a–d**,**f–i**) was developed using 3,3′-diaminobenzidine, whereas the double staining (**j–m**) used the fluorescent dyes fluorescein (green, Aβ) and rhodamine (red, Aβ43). The images in **j** and **k** are merged (yellow) in **l**. Scale bars represent 250 μm (**a–d**) and 25 μm (**f–m**). The ratio of Aβ40, Aβ42 and Aβ43 of the plaque areas in the hippocampal region of brain sections from four individuals with Alzheimer's disease were quantified in **e**. $^{**}P < 0.01$ between Aβ40 and Aβ43, one-way ANOVA with Scheffe's *F* test (see **Supplementary Fig. 15**).

the quantity of Aβ42 as well as with the age of onset of the affected individuals[24] (**Fig. 5** and **Supplementary Fig. 12**). These observations suggest that there is an intrinsic mechanism by which Aβ43 is physiologically generated and that both Aβ42 and Aβ43 may be involved in Alzheimer's disease pathogenesis. The reason for the correlation between Aβ42 and Aβ43 remains elusive.

APP × PS1-R278I versus APP × PS1-M146V mice

We generated another line of double-mutant mice by crossbreeding the APP transgenic mice with PS1-M146V knock-in mice, which served as a positive control with which to compare the APP × PS1-R278I mice, as the former mutation results in overproduction of Aβ42 rather than Aβ43 (ref. 25). As expected, the PS1-M146V mutation, unlike the PS1-R278I mutation, resulted in selective accumulation of Aβ42 (**Supplementary Fig. 13**). Although the steady-state levels of Aβ42 in the APP × PS1-M146V mice was about tenfold greater than that of Aβ43 in APP × PS1-R287I mice at 9 months, the total plaque areas, as determined by immunohistochemistry, were similar (**Fig. 6**). Both double-mutant mice accumulated Aβ40 and Aβ42, whereas Aβ43 was much more abundant in the APP × PS1-R278I mice (**Fig. 6a**,**b**). Quantitative image analyses yielded consistent results (**Fig. 6c–e**). Aβ43 immunoreactivity colocalized with the plaque cores in a manner similar to that of Aβ42, but not to that of Aβ40 (**Fig. 6f–h**). Notably, Aβ species with the third N-terminal residue converted to pyroglutamate (N3pE-Aβ), a potently pathogenic Aβ subspecies[26–29], also colocalized with plaque cores and deposits were more abundant in APP × PS1-R278I than in APP × PS1-M146V mice (**Supplementary Fig. 14**). Although the underlying mechanism that accounts for the elevated N3pE-Aβ generation in the APP × PS1-R278I mice remains unclear, the observation is consistent with a previous finding that some presenilin mutations increase the quantity of N-terminally truncated Aβ in the brains of individuals with FAD[30].

Although APP × PS1-M146V mice accumulated greater numbers of Aβ plaques in the cortical and hippocampal areas than APP × PS1-R278I mice, the density of thioflavin S-positive plaques per total plaques was significantly greater in the APP × PS1-R278I mice ($P < 0.01$; **Fig. 7a–f**). This observation indicates that Aβ43 is even more prone to seed cores in plaque formation than Aβ42. To test this hypothesis *in vitro*, we carried out thioflavin T-binding experiments using an equal amount of Aβ40, Aβ42 and Aβ43 (20 μM each). Aβ43 induced the highest incorporation of thioflavin T into Aβ aggregates (**Fig. 7g**). In addition, stoichiometric experiments, in which we added a relatively small quantity of Aβ40, Aβ42 or Aβ43 (0.2 μM) to a mixture of Aβ40 (20 μM) and Aβ42 (2 μM), revealed that, of the three, Aβ43 most potently accelerated the incorporation of thioflavin T (**Fig. 7h**). These data indicate that Aβ43 contributes to the formation of the thioflavin T-positive β-sheeted structure to a greater extent than either Aβ40 or Aβ42, a finding that may account for the observation that a relatively small amount of Aβ43 is sufficient to accelerate Aβ amyloidosis and induce plaque core formation *in vivo*.

Neural toxicity and amyloid pathology of Aβ43

Consistent with Aβ42 having higher hydrophobicity and higher toxicity than Aβ40 *in vitro* and *in vivo*, a large number of studies have found that Aβ42 contributes to synaptic dysfunctions[31–34]. We therefore compared the toxicity of Aβ40, Aβ42 and Aβ43. Aβ43 showed a higher potent neural toxicity in a dose-dependent manner as compared with Aβ40 and Aβ42 (**Fig. 7i**,**j**). These results indicate that Aβ43 directly affects neural toxicity and induces synaptic dysfunction, which would contribute to short-term memory impairments before the amyloidogenesis (**Fig. 3i**,**j**).

Finally, we performed immunohistochemical experiments on brain sections from individuals with SAD to explore the possible involvement of Aβ43 in human neuropathology. Aβ43 accumulated in the brains more frequently than Aβ40 (**Fig. 8a–e** and **Supplementary Fig. 15**), and was present in both diffuse (**Fig. 8f**,**g**) and dense-cored (**Fig. 8h**,**i**) plaques, similar to Aβ42 and N3pE-Aβ (**Supplementary Fig. 16a–d**). Furthermore, thioflavin S fluorescence signals colocalized well with Aβ43 immunoreactivity (**Fig. 8j–m**), as well as with N3pE-Aβ (**Supplementary Fig. 16e–g**). These observations are consistent with those of previous studies, which found that a substantial amount of Aβ43 accumulates in SAD and FAD brains[4–7].

DISCUSSION

Previous studies using Bri-Aβ fusion proteins have shown that Aβ42 is essential for amyloid deposition *in vivo*[31] and that Aβ40 inhibits this deposition[32]. The difference between Aβ40 and Aβ42 lies in the C-terminal amino-acid sequence, that is, the additional presence of isoleucine and alanine residues in Aβ42. Because both isoleucine and alanine are hydrophobic amino acids, it is reasonable to assume

© 2011 Nature America, Inc. All rights reserved.

that Aβ42 is more prone to form a β-sheet structure than Aβ40. In contrast, the carboxyl-terminal amino acid of Aβ43 is threonine, which carries a hydrophilic alcohol group (together with a hydrophobic methyl group) and could therefore reverse the hydrophobicity of Aβ42. Thus, the amyloidogenicity of Aβ43, a natural product of γ-secretase activity[8,9], has remained elusive.

We focused on Aβ43, an overlooked species in Alzheimer's disease research, and investigated its role in the amyloidogenesis and pathogenesis of Alzheimer's disease. To date, the major focus of research into Alzheimer's disease has been placed on the amyloidogenecity of Aβ42 and, in numerous studies, BC05, an antibody to Aβ42 that has been used to demonstrate that Aβ42 is the major pathogenic species in Alzheimer's disease. As partial crossreactivity of BC05 to Aβ43 had already been reported[35], Aβ42(43) was noted in some of the studies that used BC05. However, many studies have overestimated Aβ42 levels and ignored the possible changes in Aβ43 levels. Almost all FAD-associated PS1 mutations result in an increased Aβ42/Aβ40 ratio that is caused by an increase of Aβ42. However, some of the PS1 mutations lead to a decrease of Aβ40 with or without alteration of Aβ42 levels, which also leads to an increased Aβ42/Aβ40 ratio. One explanation of the association between decreased Aβ40 and FAD could be that Aβ40 is involved in protection from plaque fromation[32]. We found that decreased Aβ40 levels accompanied increased Aβ43 levels in PS1-R278I knock-in mice. Furthermore, the increased Aβ43 levels accelerated Aβ pathology, contributing to the early onset of the disease. Thus, we propose that Aβ43 should be separately analyzed from Aβ42.

In an effort to explore the role of Aβ43 in Aβ amyloidosis, we generated PS1-R278I knock-in mice, as this mutation causes overproduction of Aβ43 *in vitro*[13]. We chose to use this presenilin mutation knock-in procedure rather than the overexpression strategy for the following reasons. First, the R278I mutation is known to be clinically pathogenic. Second, the knock-in procedure is less artificial than transgenic overexpression approaches in general, and the knock-in mice could potentially be used to generate a relevant Alzheimer's disease model by crossbreeding with other mice, such as mutant APP transgenic or knock-in mice. Unexpectedly, the phenotype of the homozygous knock-in mice proved to be embryonic lethal in association with abnormal PS1 endoproteolysis. Limited proteolysis of APP CTF-α and CTF-β, N-cadherin, and Notch1 was also hampered in the homozygous knock-in embryos, although the γ-secretase components appeared to have been properly assembled as a 360-kDa complex. On the basis of previous studies, it appears that the disturbance in Notch1 processing represents the primary cause of the premature death that we observed[16,36]. Compared with PS1 knockout, the embryonic lethality of PS1-R278I knock-in mice occurs at a slightly later stage. Taking into account the fact that a 50% reduction of γ-secretase activity in heterozygous PS1-R278I or in heterozygous PS1 knockout mice does not lead to embryonic lethality and that a 90% reduction in homozygous PS1-R278I mice is lethal, it seems that the γ-secretase activity threshold for survival is somewhere between 10–50% of wild type. The remaining 10% γ-secretase activity in homozygous PS1-R278I knock-in mice could account for the delayed lethality compared with PS1 knockout mice (**Supplementary Fig. 10c**). Taken together, these results strongly suggested that the primary phenotype of the R278I mutation was a partial loss of function of γ-secretase activity.

Despite this, MEFs prepared from homozygous embryos produced extremely high steady-state levels of Aβ43 (approximately 20-fold greater than that of wild-type MEFs); this accompanied a substantial decrease in Aβ40 production and no changes in Aβ42 levels. Previous *in vitro* studies have found that Aβ43 is processed to Aβ40, whereas Aβ42 is independently produced from Aβ45 in the presence of γ-secretase[8,9]. Consistent with these findings, our results from crossbreeding heterozygous PS1-R278I mice with PS1 knockout mice, which showed substantial levels of both Aβ40 and Aβ43, indicate that Aβ43 was indeed converted to Aβ40 independently of Aβ42 production (**Fig. 2k**). Furthermore, we carried out *in vitro* γ-secretase assays and found that the ratio of production of Aβ46 in homozygous PS1-R278I MEFs was increased with a concomitant increase of Aβ43 and decrease of Aβ40 (**Supplementary Fig. 10**), suggesting that production of Aβ40 and Aβ43 also depends on Aβ46 production, as previously postulated[8–10]. Thus, inhibition of this Aβ43-to-Aβ40 conversion could account for the increase in Aβ43 and the concomitant decrease in Aβ40 in the knock-in MEFs. Notably, treatment of PS1-ΔE9–expressing cells with L-685,458 results in elevated Aβ43 production[37], consistent with the notion that multiple processes are involved in the generation of various Aβ species and that a partial loss of γ-secretase activity might give rise to a particular Aβ species. However, *in vitro* γ-secretase activity of heterozygous and homozygous PS1-R278I was markedly reduced in a gene dose–dependent manner, whereas there were no substantial differences in the steady-state levels of total MEF-produced Aβ compared with wild-type MEFs. To elucidate the reason behind this contradiction, it will be necessary to investigate other mechanisms, such as intracellular trafficking and secretion of Aβ, in depth.

The molecular mechanism that allows Aβ43 production, but not other proteolytic processes, remains to be clarified, but it likely involves specific conformational changes of the γ-secretase complex[38]. Because Aβ42 is produced independently of Aβ43 in the presence of γ-secretase, some of the FAD-associated PS1 mutations that cause a decrease in Aβ40 without an increase in Aβ42, such as A79V, A231V, C263F, L282V, L166P and G384A[24,39], might actually result in the elevation of Aβ43 in a manner similar to the R278I mutation. In addition, PS1-ΔE10, an artificial PS1 mutation located to the loop domain of PS1 where R278I is present, leads to a substantial reduction of the steady-state levels of Aβ40 without any alteration of Aβ42 levels, similar to our results; however, Aβ43 levels were not measured[40]. It will therefore be important to investigate whether these FAD-associated mutations give rise to increased Aβ43 levels and to scrutinize their amyloidogenicity. In fact, the I143T, L262F, L282V and G384A mutations did lead to substantial production of Aβ43 in our transfection assays. Notably, Aβ43 levels and the ratio of Aβ43/Aβ40 substantially correlated well with the age of disease onset in a manner similar to Aβ42 levels and the ratio of Aβ42/Aβ40. In addition, a PS1-I143T carrier in a Swedish family with FAD gave rise to high levels of Aβ43 (ref. 7). These observations highlight the possibility that compounds that facilitate the Aβ43-to-Aβ40 and Aβ42-to-Aβ38 conversions might be beneficial for prevention and treatment of Alzheimer's disease by decreasing both Aβ42 and Aβ43. In support of this notion, an oral vaccination with an adeno-associated virus vector carrying Aβ1–43 cDNA was reported to result in a marked reduction of Aβ burdens and improvement of behavioral performances in Tg2576 APP transgenic mice[41,42].

Although we originally thought to generate APP × homozygous PS1-R278I mice, we also explored the possible utility of heterozygous PS1-R278I knock-in mice, given that overexpression of APP in heterozygous PS1-R278I knock-in MEFs resulted in selective elevation of Aβ43. Consistent with this, APP × heterozygous PS1-R278I mice exhibited short-term memory impairment, selective biochemical accumulation of Aβ43 at an early stage before plaque formation and substantial acceleration of Aβ pathology thereafter as compared with APP mice. It should also be noted that the APP × PS1-R278I mice

© 2011 Nature America, Inc. All rights reserved. npg

exhibited a greater density of the thioflavin S–positive signal per plaque than APP × PS1-M146V mice, which overproduced Aβ42 instead of Aβ43. Consistent with previous reports[6,7], we observed Aβ43-positive plaques more often than Aβ40-positive ones in the brains of individuals with Alzheimer's disease. Aβ43 has previously been found in amyloid plaques in individuals with Alzheimer's disease[4,6,7], as well as in aged gorillas[43] and in some Alzheimer's disease model mice harboring PS1 or APP FAD mutations[3,10]. In addition, it has been suggested that the amount of Aβ43 in plaques correlates with cognitive decline[5]. We also found that Aβ43 exhibited potent neural toxicity, comparable to or even greater than that of Aβ42. These findings establish that Aβ43 is indeed amyloidogenic *in vivo* and likely to be pathogenic. Thus, the C-terminal amino acid residue of Aβ43, threonine, appears to strengthen the hydrophobicity of the peptide rather than reversing it.

Notably, biochemical accumulation of Aβ43 preceded pathological deposition in the APP × PS1-R278I mice and in the single APP mice. In addition, the basal Aβ43 levels substantially increased with aging in wild-type mice up to at least 18 months of age (data not shown). These observations suggest that Aβ43 is potentially valuable as a biomarker for presymptomatic diagnosis of Alzheimer's disease. We believe that it would be worth trying to quantify Aβ43 levels in cerebrospinal fluid from individuals with Alzheimer's disease and controls. We also detected the presence of N3pE-Aβ in APP × PS1-R278I mouse brains, a finding that is supported by a previous report quantitatively describing N3pE-Aβ42 and N3pE-Aβ43 in the brains of individuals with FAD or SAD[2]. It is of particular interest that Pittsburgh Compound B, a probe for amyloid imaging by positron emission tomography, selectively binds to N3pE-Aβ[26], implying that N3pE-Aβ42/43 could be particularly prone to seed deposition of other Aβ species, consistent with previous findings[28]. It is also possible that the mutation might affect the interaction of PS1 with other substrates or alter its property of non-γ-secretase activity, such as regulation of neurotransmitter release[29].

In summary, our results indicate that Aβ43, which has largely been overlooked, is potently amyloidogenic and toxic, and highlight the potential value of Aβ43, that is, cerebrospinal fluid Aβ43 levels, as an early marker for some of the detrimental effects of aging in the adult brain. We propose that inhibition of Aβ43 generation, such as by facilitating the conversion of Aβ43 to Aβ40 in the γ-secretase complex, should be beneficial for prevention of Aβ amyloidosis.

METHODS

Methods and any associated references are available in the online version of the paper at http://www.nature.com/natureneuroscience/.

Note: Supplementary information is available on the Nature Neuroscience website.

ACKNOWLEDGMENTS

We thank M.N. Rossor (University College London) for sharing clinical information about the R278I mutation carriers, J.Q. Trojanowski and V.M.-Y. Lee (University of Pennsylvania) for providing postmortem brain tissues, R. Kopan (Washington University) for providing Myc-tagged ΔNotch1 plasmid, A. Takashima (RIKEN Brain Science Institute) for providing antibody to Aph-1, and J. Hardy (University College London) for valuable discussions. This work was supported by research grants from RIKEN Brain Science Institute, the Ministry of Education, Culture, Sports, Science and Technology, the Ministry of Health, Labor and Welfare of Japan, the TAKEDA Science Foundation, the Fund for Scientific Research - Flanders (FWO-V), the Interuniversity Attraction Poles program P6/43 of the Belgian Federal Science Policy Office and a Methusalem Excellence Grant of the Flemish Government to C.V.B. N.B receives a FWO-V postdoctoral fellowship.

AUTHOR CONTRIBUTIONS

This study was jointly designed by T. Saito, T. Suemoto and T.C.S. Experiments were performed by T. Saito, T. Suemoto, N.M., Y.M., K.Y. and S.F. T. Saito, T. Suemoto, S.F., K.Y., P.N., J.T., M.N., N.I., C.V.B., Y.I. and T.C.S. jointly analyzed and interpreted data. N.B., K.S. and C.V.B. identified pathogenic PS1 mutations in patients and families and generated *PSEN1* vector constructs for expression studies.

COMPETING FINANCIAL INTERESTS

The authors declare no competing financial interests.

Published online at http://www.nature.com/natureneuroscience/.
Reprints and permissions information is available online at http://www.nature.com/reprints/index.html.

1. Blennow, K., de Leon, M.J. & Zetterberg, H. Alzheimer's disease. *Lancet* **368**, 387–403 (2006).
2. Miravalle, L. *et al.* Amino-terminally truncated Aβ peptide species are the main component of cotton wool plaques. *Biochemistry* **44**, 10810–10821 (2005).
3. Van Vickle, G.D. *et al.* TgCRND8 amyloid precursor protein transgenic mice exhibit an altered γ-secretase processing and an aggressive, additive amyloid pathology subject to immunotherapeutic modulation. *Biochemistry* **46**, 10317–10327 (2007).
4. Iizuka, T. *et al.* Amyloid β-protein ending at Thr43 is a minor component of some diffuse plaques in the Alzheimer's disease brain, but is not found in cerebrovascular amyloid. *Brain Res.* **702**, 275–278 (1995).
5. Parvathy, S. *et al.* Correlation between Aβx-40-, Aβx-42- and Aβx-43-containing amyloid plaques and cognitive decline. *Arch. Neurol.* **58**, 2025–2032 (2001).
6. Welander, H. *et al.* Aβ43 is more frequent than Aβ40 in amyloid plaque cores from Alzheimer disease brains. *J. Neurochem.* **110**, 697–706 (2009).
7. Keller, L. *et al.* The *PSEN1* I143T mutation in a Swedish family with Alzheimer's disease: clinical report and quantification of Aβ in different brain regions. *Eur. J. Hum. Genet.* **18**, 1202–1208 (2010).
8. Qi-Takahara, Y. *et al.* Longer forms of amyloid β protein: implications for the mechanism of intramembrane cleavage by γ-secretase. *J. Neurosci.* **25**, 436–445 (2005).
9. Takami, M. *et al.* γ-Secretase: successive tripeptide and tetrapeptide release from the transmembrane domain of β-carboxyl terminal fragment. *J. Neurosci.* **29**, 13042–13052 (2009).
10. Shimojo, M. *et al.* Enzymatic characteristics of I213T mutant Presenilin-1/γ-secretase in cell models and knock-in mouse brains: FAD-linked mutation impairs γ-site cleavage of APP-CTFβ. *J. Biol. Chem.* **283**, 16488–16496 (2008).
11. Jarrett, J.T., Berger, E.P. & Lansbury, P.T. Jr. The carboxy terminus of the β amyloid protein is critical for the seeding of amyloid formation: implications for the pathogenesis of Alzheimer's disease. *Biochemistry* **32**, 4693–4697 (1993).
12. Bitan, G. *et al.* Amyloid β-protein (Aβ) assembly: Aβ40 and Aβ42 oligomerize through distinct pathways. *Proc. Natl. Acad. Sci. USA* **100**, 330–335 (2003).
13. Nakaya, Y. *et al.* Random mutagenesis of presenilin-1 identifies novel mutants exclusively generating long amyloid β-peptides. *J. Biol. Chem.* **280**, 19070–19077 (2005).
14. Godbolt, A.K. *et al.* A presenilin 1 R278I mutation presenting with language impairment. *Neurology* **63**, 1702–1704 (2004).
15. Shen, J. *et al.* Skeletal and CNS defects in Presenilin-1-deficient mice. *Cell* **89**, 629–639 (1997).
16. Wong, P.C. *et al.* Presenilin 1 is required for Notch1 and Dll1 expression in the paraxial mesoderm. *Nature* **387**, 288–292 (1997).
17. Culvenor, J.G. *et al.* Characterization of presenilin complexes from mouse and human brain using blue native gel electrophoresis reveals high expression in embryonic brain and minimal change in complex mobility with pathogenic presenilin mutations. *Eur. J. Biochem.* **271**, 375–385 (2003).
18. Evin, G. *et al.* Transition-state analogue γ-secretase inhibitors stabilize a 900 kDa presenilin/nicastrin complex. *Biochemistry* **44**, 4332–4341 (2005).
19. Thinakaran, G. *et al.* Endoproteolysis of presenilin 1 and accumulation of processed derivatives *in vivo*. *Neuron* **17**, 181–190 (1996).
20. Lee, M.K. *et al.* Hyperaccumulation of FAD-linked presenilin 1 variants *in vivo*. *Nat. Med.* **3**, 756–760 (1997).
21. Kaneko, H. *et al.* Enhanced accumulation of phosphorylated α-synuclein and elevated β-amyloid 42/40 ratio caused by expression of the presenilin-1 ΔT440 mutant associated with familial Lewy body disease and variant Alzheimer's disease. *J. Neurosci.* **27**, 13092–13097 (2007).
22. Schroeter, E.H. *et al.* A presenilin dimer at the core of the γ-secretase enzyme: insight from parallel analysis of Notch1 and APP proteolysis. *Proc. Natl. Acad. Sci. USA* **100**, 13075–13080 (2003).
23. Hama, E., Shirotani, K., Iwata, N. & Saido, T.C. Effects of neprilysin chimeric proteins targeted to subcellular compartments on amyloid β peptide clearance in primary neurons. *J. Biol. Chem.* **279**, 30259–30264 (2004).
24. Kumar-Singh, S. *et al.* Mean age-of-onset of familial Alzheimer disease caused by presenilin mutations correlates with both increased Aβ42 and decreased Aβ40. *Hum. Mutat.* **27**, 686–695 (2006).
25. Wang, R., Wang, B., He, W. & Zheng, H. Wild-type presenilin 1 protects against Alzheimer disease mutation-induced amyloid pathology. *J. Biol. Chem.* **281**, 15330–15336 (2006).
26. Maeda, J. *et al.* Longitudinal, quantitative assessment of amyloid, neuroinflammation, and anti-amyloid treatment in a living mouse model of Alzheimer's disease enabled by positron emission tomography. *J. Neurosci.* **27**, 10957–10968 (2007).

© 2011 Nature America, Inc. All rights reserved. npg

27. Saido, T.C. *et al.* Dominant and differential deposition of distinct β-amyloid peptide species, AβN3(pE), in senile plaques. *Neuron* **14**, 457–466 (1995).
28. Schilling, S. *et al.* Glutaminyl cyclase inhibition attenuates pyroglutamate Aβ and Alzheimer's disease–like pathology. *Nat. Med.* **14**, 1106–1111 (2008).
29. Zhang, C. *et al.* Presenilins are essential for regulating neurotransmitter release. *Nature* **460**, 632–636 (2009).
30. Russo, C. *et al.* Presenilin-1 mutations in Alzheimer's disease. *Nature* **405**, 531–532 (2000).
31. McGowan, E. *et al.* Aβ42 is essential for parenchymal and vascular amyloid deposition in mice. *Neuron* **47**, 191–199 (2005).
32. Kim, J. *et al.* Aβ40 inhibits amyloid deposition in vivo. *J. Neurosci.* **27**, 627–633 (2007).
33. Ono, K., Condron, M. & Teplow, D.B. Effects of the English (H6R) and Tottori (D7N) familial Alzheimer disease mutations on amyloid β-protein assembly and toxicity. *J. Biol. Chem.* **285**, 23186–23197 (2010).
34. Jan, A. *et al.* The ratio of monomeric to aggregated forms of Aβ40 and Aβ42 is an important determinant of amyloid-β aggregation, fibrillogenesis, and toxicity. *J. Biol. Chem.* **283**, 28176–28189 (2008).
35. Huppert, S.S. *et al.* Embryonic lethality in mice homozygous for a processing-deficient allele of Notch1. *Nature* **405**, 966–970 (2000).
36. Ikeuchi, T. *et al.* Familial Alzheimer disease-linked presenilin 1 variants enhance production of both Aβ1–40 and Aβ1–42 peptides that are only partially sensitive to a potent aspartyl protease transition state inhibitor of "γ-secretase". *J. Biol. Chem.* **278**, 7010–7018 (2003).
37. Serneels, L. *et al.* γ-Secretase heterogeneity in the Aph1 subunit: relevance for Alzheimer's disease. *Science* **324**, 639–642 (2009).
38. Bentahir, M. *et al.* Presenilin clinical mutations can affect γ-secretase activity by different mechanisms. *J. Neurochem.* **96**, 732–742 (2006).
39. Deng, Y. *et al.* Deletion of presenilin 1 hydrophilic loop sequence leads to impaired γ-secretase activity and exacerbated amyloid pathology. *J. Neurosci.* **26**, 3845–3854 (2006).
40. Hara, H. *et al.* Development of a safe oral Aβ vaccine using recombinant adeno-associated virus vector for Alzheimer's disease. *J. Alzheimers Dis.* **6**, 483–488 (2004).
41. Mouri, A. *et al.* Oral vaccination with a viral vector containing Aβ cDNA attenuates age-related Aβ accumulation and memory deficits without causing inflammation in a mouse Alzheimer model. *FASEB J.* **21**, 2135–2148 (2007).
42. Kimura, N. *et al.* Senile plaques in an aged Western Lowland Gorilla. *Exp. Anim.* **50**, 77–81 (2001).
43. Sturchler-Pierrat, C. *et al.* Two amyloid precursor protein transgenic mouse models with Alzheimer disease–like pathology. *Proc. Natl. Acad. Sci. USA* **94**, 13287–13292 (1997).
44. Huang, S.-M. *et al.* Neprilysin-sensitive synapse-associated amyloid-β peptide oligomers impair neuronal plasticity and cognitive function. *J. Biol. Chem.* **281**, 17941–17951 (2006).

© 2011 Nature America, Inc. All rights reserved.
npg

ONLINE METHODS

Generation of PS1-R278I knock-in mice. The genomic DNA of mouse *PSEN1* was isolated from the bacterial artificial chromosome (BAC) library from the 129/Sv mouse genome, and one BAC clone that included introns 5–11 of the *PSEN1* gene was obtained (**Supplementary Fig. 1**). The fragment from the ApaI site of intron 5 to the HindIII site of intron 11 provided the basis for construction of the targeting vector. To introduce the PS1-R278I mutation, we subcloned the SmaI/BamHI fragment containing introns 7 and 8 of the *PSEN1* gene into pBluescript vector. To introduce the R278I mutation, we used 5′-GGT TGA AAC AGC TCA GGA AA<u>T</u> AAA TGA GAC TCT CTT TCC AGC-3′ (underlined, original G to T mutation) as our primer, using GeneEditor Mutagenesis System (Promega) according to the manufacturer's protocol. This fragment was used to replace the original sequence of the *PSEN1* gene. Finally, a *pgk-neo* gene cassette was inserted for positive selection at the EcoRI/SmaI sites located in intron 7, and a diphtheria toxin A fragment cassette was inserted for negative selection at the HindIII site in intron 11. We used the ApaI/EcoRI fragment spanning from intron 5 to intron 7 (4.3 kb) as the long arm and the BamHI/HindIII fragment spanning from intron 8 to intron 11 (3.8 kb) as the short arm of the targeting vector.

Embryonic stem cell cultures and gene-targeting experiments were carried out as described previously. Targeted embryonic stem cells were microinjected into 129/Sv blastocysts. DNA was extracted from the biopsied tail of mouse pups, and the F1 generation of the mutant animals was identified by Southern blot analysis with a 3′ external probe that was produced by PCR using 5′-AAT GGA TAA TCA GAG CCT GCC-3′ and 5′-TCC TCA CAA CTA ACT ACC CAA GG-3′ as primers.

The heterozygous mice were crossbred with EIIa-Cre transgenic mice to remove the *pgk-neo* gene, after which the generated PS1-R278I knock-in mice were backcrossed to the C57BL6/J strain. When the *pgk-neo* gene was removed by Cre excision, a short sequence ranging from the EcoRI to the SmaI sites of intron 7 was also removed. Deletion of this short sequence in intron 7 enables detection of the genotype of mutant mice. To genotype the PS1-R278I knock-in mouse, tail DNA was isolated and subjected to PCR analysis using 5′-AGT TTC AGA CCA GCC TAG GCC AC-3′ and 5′-AGG AAG GGA GAC TTG ACA GC-3′ as primers.

Other mutant mice. PS1 knockout mice and PS1-M146V knock-in mice were purchased from the Jackson Laboratory. APP23 mice carrying the human APP isoform 751 transgene harboring the Swedish mutation (K651N M652L)[45] have been described previously[46]. All animal experiments were carried out according to the RIKEN Brain Science Institute's guidelines for animal experimentation.

MEFs. MEFs were prepared from E13–14 embryos of wild-type, PS1-R278I knock-in and PS1 knockout mice, and inoculated in Dulbecco's modified Eagle medium supplemented with 10% fetal bovine serum (FBS, vol/vol). The conditioned medium and cell lysates from MEFs (passage <8) were subjected to biochemical analyses, including ELISA, native PAGE and western blotting. Transfection of the MEFs with the Myc-tagged ΔNotch construct[47] was performed using FuGENE 6 Transfection Reagent (Roche) according to the manufacturer's instructions.

Blue native-PAGE (BN-PAGE). Non-denaturing native PAGE was performed to confirm the integrity of the γ-secretase complexes[17] using the Novex Bis-Tris gel system (Invitrogen) according to the manufacturer's instructions. Samples were extracted from embryonic brains and MEFs using the sample buffer from the Novex Bis-Tris gel system that contains 1% digitonin. Equal amounts of proteins as determined using the BCA Protein Assay Kit (Pierce) were loaded on a 3–12% gradient Bis-Tris acrylamide gel. Immunoblotting was performed using the antibodies H70 (to the PS1 N terminus, Santa Cruz) and Ab-2 (to PS2, Calbiochem).

Immunoprecipitation assay and western blot analysis. Brain homogenates from embryonic brains (E14–16) and cell lysates of MEFs were immunoprecipitated with H70, and then captured by Dynabead-conjugating protein G (Invitrogen). Immunoprecipitants were subjected to western blot analysis using antibodies H70, MAB5232 (to the PS1 loop, Chemicon), Ab-2, PA1-758 (to Nicastrin, Affinity Bioreagents) and ACS-01 (to Aph1)[10], and antibody to Pen-2 (Zymed). In addition, we used antibody to Aβ1-12 (6E10, Covance), antibody to the N terminus of APP (22C11, Chemicon), antibody to APP CTF (Sigma), antibody to Myc (9B11, Cell Signaling), antibody to Notch1 (mN1A, BD Bioscience) and antibody to β-actin (AC-15, Sigma).

ELISA. Soluble materials from mouse cortical hemispheres were dissolved in Tris-HCl–buffered saline and the insoluble materials were dissolved in guanidine-HCl solution as described previously[48]. Samples from the brains and from the conditioned medium of MEFs were analyzed using an Aβ-ELISA kit (Wako) to quantify Aβ40. To specifically quantify the levels of Aβ42 and Aβ43, we established an Aβ42- and Aβ43-specific sandwich ELISA system using the Aβ-ELISA kit (Wako). Given that BC05, a detection antibody of this kit, cross-reacts with Aβ42 and Aβ43 (ref. 35), we used the Aβ42- and Aβ43-specific antibodies C42 (Aβ42 specific, IBL) and C43 (Aβ43 specific, IBL). The specificities of these antibodies are shown in **Figure 2c–e** and **Supplementary Figure 6c–e**. Samples were incubated overnight at 4 °C in a 96-well plate coated with the capture antibody, BNT77 (antibody to Aβ11–28)[49]. Aβ from samples captured in the ELISA were incubated with C42 or C43 (1:100, 3 h at 20–25 °C), after which horseradish peroxidase–conjugated antibody to rabbit IgG (1:500, 2 h at 20–25 °C) was added as a detection antibody. Synthesized Aβ42 or Aβ43 peptide (Peptide Institute) was used for the preparation of a standard curve, and diluted with the diluents solutions provided in the kit. For consistency, when we quantified the amount of Aβ40, a synthesized Aβ40 peptide (Peptide Institute) was also used for the preparation of a standard curve. This system also worked in broader concentration range of Aβ42 and Aβ43 (**Supplementary Fig. 6a,b**). Furthermore, a highly sensitive Aβ43 system, based on modified protocols, was established for the measurement of samples containing small amounts of Aβ43, such as samples derived from non–APP transgenic mice and cells that are not overexpressing APP (**Supplementary Fig. 7**).

Immunohistochemical and histochemical studies. Paraffin-embedded mouse brain sections were immunostained with 4G8 (antibody to Aβ17-24, Covance), C40 (specific antibody to Aβ40, IBL), C42, C43 and MAB3402 (antibody to GFAP, Chemicon), with or without tyramide signal amplification (PerkinElmer Life Sciences) as described previously[48]. Quantification of immunoreactivity from brain sections were carried out using MetaMorph imaging software (Universal Imaging) as previously described[48].

Y-maze test. Mice were housed individually before transferring to the behavioral laboratory. They were kept during the behavioral analysis. The light condition was 12-h:12-h (lights on 8:00). The laboratory was air-conditioned and maintained at a temperature of approximately 22–23 °C and a humidity of approximately 50–55%. Food and water were freely available except during experimentation. Large tweezers were used to handle mice to avoid individual differences in the handling procedure. All of the experiments were conducted in the light phase (9:00–18:00), and the starting time of the experiments was kept constant.

The Y-maze apparatus (O'Hara) was made of gray plastic and consisted of three compartments (3-cm (width) bottom and 10-cm (width) top, 40 cm (length) and 12 cm (height)) radiating out from the center platform (3 × 3 × 3 cm triangle). The maze was positioned 80 cm above the floor, surrounded by a number of desks and test apparatuses around the maze to act as spatial cues. In this test, each mouse was placed in the center of the maze facing toward one of the arms and was then allowed to explore freely for 5 min. Experiments were performed at a light intensity of 150 lx at the platform. An arm entry was defined as four legs entering one of the arms, and the experimenter counted the sequence of entries by watching a TV monitor behind a partition. An alternation was defined as entry into all three arms on consecutive choices (the maximum number of alternations was the total number of entries minus 2). The percent alternation was calculated as (actual alternations divided by maximum alternations) × 100. The percent alternation was designated as the spontaneous alternation behavior of the mouse, was taken as a measure of memory performance.

Thioflavin T–binding assay. The thioflavin T–binding assay was performed by mixing aliquots of Aβ. Human Aβ1–40, Aβ 1–42 and Aβ1–43 were purchased from the Peptide Institute. We first examined the aggregation properties of Aβ40, Aβ42 and Aβ43 individually by incubating the peptides separately at 20 μM in 50 mM potassium phosphate buffer (pH 7.4) at 37 °C for 24 h with agitation. The stoichiometric effect of different Aβ species on aggregation was investigated in

© 2011 Nature America, Inc. All rights reserved.

the mixture of Aβ40 and Aβ42 by adding and mixing Aβs in 50 mM potassium phosphate buffer (pH 7.4) at molar concentrations of 20:2:0.2 μM (Aβ40:Aβ42: Aβ40, Aβ42 or Aβ43 = 100:10:1) and incubating them at 37 °C for 24 h with agitation. After incubation, thioflavin T was added to a final concentration of 5 μM and thioflavin T fluorescence was measured at excitation and emission wavelengths of 442 nm and 485 nm, respectively.

Neural cell toxicity assay. Primary cortical neurons were isolated as previously described[23] and plated at a density of 5×10^4 cells per well in 96-well plate ($n = 6$ wells in each experimental conditions). We treated 10–14 d *in vitro* cultures with synthesized Aβ40, Aβ42 and Aβ43 peptide (Peptide Institute) at 0.1 to 10 μM of Aβs for 72 h. These Aβ peptides were dissolved in 10 mM phosphate buffer (pH 7.4, 90%) and 60 mM NaOH (10%), which was used as the vehicle[33]. SH-SY5Y cells were plated at a density of 2×10^4 cells per well with 10% FBS supplemented medium in 96-well plate ($n = 6$ wells in each experimental conditions), and incubated for 24 h. Then the medium was replaced with medium containing 1% FBS (vol/vol), and treated with each Aβ peptides for 48 h. Cell viability was determined using MTS assay (CellTiter 96 Aqueous One Solution Cell Proliferation Assay Kit, Promega)[50], and lactate dehydrogenase release as cell toxicity was performed using CytoTox-ONE Homogeneous Membrane Integrity Assay Kit (Promega)[33], according to the manufacturer's instructions and compared to vehicle treated cells.

Alzheimer's disease brain sections. Post-mortem Alzheimer's disease brain tissues were kindly provided by J.Q. Trojanowski and V.M.-Y. Lee (University of Pennsylvania). The tissues had been fixed with ethanol or formalin and embedded in paraffin. This study was approved by the Institutional Review Board of the RIKEN Brain Science Institute.

45. Kopan, R., Schroeter, E.H., Weintraub, H. & Nye, J.S. Signal transduction by activated mNotch: importance of proteolytic processing and its regulation by the extracellular domain. *Proc. Natl. Acad. Sci. USA* **93**, 1683–1688 (1996).
46. Iwata, N. *et al.* Presynaptic localization of neprilysin contributes to efficient clearance of amyloid-β peptide in mouse brain. *J. Neurosci.* **24**, 991–998 (2004).
47. Iwatsubo, T. *et al.* Visualization of Aβ42(43) and Aβ40 in senile plaques with end-specific Aβ monoclonals: evidence that an initially deposited species is Aβ42(43). *Neuron* **13**, 45–53 (1994).
48. Enya, M. *et al.* Appearance of sodium dodecylsulfate-stable amyloid β-protein (Aβ) dimer in the cortex during aging. *Am. J. Pathol.* **154**, 271–279 (1999).
49. Ryan, D.A., Narrow, W.C., Federoff, H.J. & Bowers, W.J. An improved method for generating consistent soluble amyloid-beta oligomer preparations for *in vitro* neurotoxicity studies. *J. Neurosci. Res.* **190**, 171–179 (2010).
50. Arango, D. *et al.* Systemic genetic study of Alzheimer disease in Latin America: mutation frequencies of the amyloid β precursor protein and presenilin gene in Colombia. *Am. J. Med. Genet.* **103**, 138–143 (2001).

© 2011 Nature America, Inc. All rights reserved.

doi:10.1038/nn.2858

Behavioral/Systems/Cognitive

ERK2 Contributes to the Control of Social Behaviors in Mice

Yasushi Satoh,[1] Shogo Endo,[5] Takahiro Nakata,[2] Yasushi Kobayashi,[2] Kazuyuki Yamada,[6] Toshio Ikeda,[7] Atsuya Takeuchi,[3] Takeshi Hiramoto,[4] Yasuhiro Watanabe,[4] and Tomiei Kazama[1]

Departments of [1]Anesthesiology, [2]Anatomy and Neurobiology, [3]Ophthalmology, and [4]Pharmacology, National Defense Medical College, 359-8513 Tokorozawa, Japan, [5]Aging Regulation Research Team, Tokyo Metropolitan Geriatric Hospital and Institute of Gerontology, 173-0015 Tokyo, Japan, [6]Research Resources Center, RIKEN Brain Science Institute, 351-0198 Wako, Japan, and [7]Laboratory of Experimental Animal Model Research, National Center for Geriatrics and Gerontology, 474-8511 Obu, Japan

Signaling through extracellular signal-regulated kinase (ERK) is important in multiple signal transduction networks in the CNS. However, the specific role of ERK2 in *in vivo* brain functions is not fully understood. Here we show that ERK2 play a critical role in regulating social behaviors as well as cognitive and emotional behaviors in mice. To study the brain function of ERK2, we used a conditional, region-specific, genetic approach to target *Erk2* using the Cre/loxP strategy with a *nestin* promoter-driven *cre* transgenic mouse line to induce recombination in the CNS. The resulting *Erk2* conditional knock-out (CKO) mice, in which *Erk2* was abrogated specifically in the CNS, were viable and fertile with a normal appearance. These mice, however, exhibited marked anomalies in multiple aspects of social behaviors related to facets of autism-spectrum disorders: elevated aggressive behaviors, deficits in maternal nurturing, poor nest-building, and lower levels of social familiarity and social interaction. *Erk2* CKO mice also exhibited decreased anxiety-related behaviors and impaired long-term memory. Pharmacological inhibition of ERK1 phosphorylation in *Erk2* CKO mice did not affect the impairments in social behaviors and learning disabilities, indicating that ERK2, but not ERK1 plays a critical role in these behaviors. Our findings suggest that ERK2 has complex and multiple roles in the CNS, with important implications for human psychiatric disorders characterized by deficits in social behaviors.

Introduction

The extracellular signal-regulated kinase (ERK) cascade links transmembrane receptors to downstream effector mechanisms. In neurons, the ERK cascade is activated by stimuli associated with synaptic activity, and in turn activated ERK phosphorylates numerous proteins involved in a diverse array of cellular processes including long-term potentiation, long-term depression, synaptogenesis, and transcriptional and translational regulation (Kelleher et al., 2004; Thomas and Huganir, 2004). Although numerous studies have investigated the role of ERKs in behavioral plasticity, it is controversial whether the ERK isoforms, ERK1 and ERK2, redundantly share their many brain functions and compensate for each other or whether they play distinctive roles. In the analysis of ERK signaling, most experiments use inhibitors of the upstream kinase, MEK. ERK1 and 2 are solely activated by MEK, and thus, it is difficult to examine the specific contribution of each isoform to physiological functions.

Received May 11, 2011; revised June 14, 2011; accepted June 20, 2011.

Author contributions: Y.S. designed research; Y.S., S.E., T.N., Y.K., and A.T. performed research; Y.S., S.E., K.Y., T.I., T.H., Y.W., and T.K. analyzed data; Y.S. and S.E. wrote the paper.

This study was in part performed with support from the Ministry of Education, Culture, Sports, Science and Technology of Japan, the Naito Foundation, and Japan Foundation for Aging and Health. We thank Masako Suzuki, Yuko Ogura, and Kiyoko Takamiya for their excellent technical help; Yayoi Ichiki for her technical assistance in the electron microscopic study, Dr. Kouichi Fukuda for his assistance in animal administration, and Drs. Yuki Takayanagi, Tadashi Kimura, and Kenichi Furuya for advice on the study of maternal behaviors. The *nestin-cre* transgenic mice were a kind gift from Dr. R. Kageyama (University of Kyoto).

Correspondence should be addressed to Dr. Yasushi Satoh, Department of Anesthesiology, National Defense Medical College, 3-2 Namiki, 359-8513 Tokorozawa, Japan. E-mail: ys@ndmc.ac.jp.

DOI:10.1523/JNEUROSCI.2349-11.2011

Copyright © 2011 the authors 0270-6474/11/3111953-15$15.00/0

Recently, however, accumulating evidence has suggested that the role of each isoform in long-term memory may not be functionally redundant. It was demonstrated that *Erk1* knock-out mice did not show a significant impairment in learning ability (Selcher et al., 2001), although the treatment of rodents with a MEK inhibitor impaired memory formation (Kelleher et al., 2004; Thomas and Huganir, 2004). On the other hand, we reported that *Erk2* knockdown mice, in which *Erk2* expression was partially (20–40%) reduced, showed deficits in long-term memory (Satoh et al., 2007).

Although these results suggest a central contribution of the ERK2 isoform to learning and memory, a specific role of ERK2 for other behavioral profile has not been fully revealed *in vivo*. However, accumulating evidence has suggested that the ERK pathway is also involved in regulating emotional/affective behaviors (Ailing et al., 2008; Engel et al., 2009) potentially as an integrator at the nexus of multiple neuronal signaling cascades. Moreover, the relevance of ERK to human psychiatric disorder has been speculated (Kumar et al., 2008; Engel et al., 2009). Considering the complex and pleiotropic involvement of ERK in neuronal functions, it is important to examine the behavioral profile of *Erk2* conditional knock-out (CKO) mice in detail and dissect the roles of ERK1 and ERK2 to understand the clinical relevance.

Because *Erk2* knock-out is embryonically lethal (Satoh et al., 2007), the conditional loss of *Erk2* in the nervous system is of great interest to gain a better understanding of the specific functions of ERK2 *in vivo*. Here, we used a conditional, region-specific, genetic approach to target *Erk2* using the Cre/loxP

strategy with a *nestin* promoter-driven *cre* transgenic mouse line, in which *cre* activity is confined to the CNS.

We found that *Erk2* CKO mice exhibited marked anomalies in social behaviors as well as decreased anxiety-related behaviors and deficits in long-term memory. These anomalies have great relevance to autism-spectrum disorders (ASDs). Our findings suggest pleiotropic roles for ERK2 in neurological and behavioral functions, and that this protein might be a factor underlying human psychiatric disorders.

Materials and Methods

Mice. All experiments were conducted according to the institutional ethical guidelines for animal experiments and the safety guidelines for gene manipulation experiments of the National Defense Medical College and were approved by the Committee for Animal Research at the National Defense Medical College (Tokorozawa, Saitama, Japan). Mice were maintained on a 12 h light-dark cycle (lights on from 7:00 A.M. to 7:00 P.M.) with room temperature at 21 ± 1°C. Mice had *ad libitum* access to water and food.

Generation of floxed Erk2 *and* Erk2 *CKO mice.* The *Erk2* gene was isolated from a 129X1/SvJ mouse genomic library. To generate the *Erk2*(floxN) allele, we constructed a targeting vector from 16.8 kb of *Erk2* DNA (from the ApaI site in intron 1 to the TaqI site in intron 6) (Fig. 1*A*). For positive selection, a floxed (flanked by loxP sites) *Pgk-neo* cassette was inserted in the opposite direction into the EcoRI site in intron 1. A third *loxP* site, KpnI, and SapI sites were inserted into the BglII site in intron 3 (Fig. 1*A*). Targeted insertion of the plasmid by homologous recombination was performed in 129 derived embryonic stem cells (E14), and derived germline targeted offspring ($Erk2^{+/flox(Neo+)}$ mice) were obtained. While the expression of ERK2 in $Erk2^{flox(Neo+)/flox(Neo+)}$ mice was reduced owing to the presence of the *Pgk-neo* cassette (Satoh et al., 2007), it resumed normal levels after excision of the neo cassette by *in vivo* crossing with transgenic mice expressing *cre* recombinase (EIIA-*cre* mice) to obtain mice carrying the *Erk* (*flox(Neo⁻)*) allele ($Erk2^{+/flox(Neo-)}$ mice) or the *Erk2* (*Δflox*) allele ($Erk2^{+/\Delta flox}$ mice). The disruption of the *Erk2* gene locus was confirmed by Southern blot analysis of genomic DNA from adult mice (Fig. 1*B*,*C*). In the genotyping PCR, the primers used for detection of the *Erk2*(flox) and *Erk2* wild-type alleles were mE2-F3 (5′-GATCTGATGCTTGCCAAAGCC-3′) and mE2-R4 (5′-TGTAAAGTAGCAGCAGATGC-3′) (Fig. 1*D*). The primers used for detection of the *Erk2*(Δflox) allele were mE2-F3 and mE2-R1 (5′-CAGAGTTTCATTATGGAGTCCTCGC-3′) (Fig. 1*D*).

$Erk2^{+/flox(Neo-)}$ mice were backcrossed with C57BL/6J mice for >10 generations. We crossed these mice with *nestin* promoter-driven *cre* transgenic mice (Vernay et al., 2005), which were maintained on the same background (C57BL/6J).

Electron microscopy. Electron microscopy was performed as previously described (Nakata and Yorifuji, 1999). Briefly, under deep anesthesia by intraperitoneal injection of pentobarbital (50 mg/kg), mice (7-weeks of age) were perfused transcardially with 0.1% heparin-PBS followed by a fixative with 2.5% glutaraldehyde, 2% paraformaldehyde in 0.1 M phosphate buffer, pH 7.4. The brains were immediately removed from the skull and cut into coronal slices (1 mm thick). Under a stereomicroscope, small pieces (1 × 1 mm) of the slices were extracted from the hippocampal CA1 or layer II/III of the temporal association cortex (at the levels 2.0 mm caudal to bregma). Then, semithin (200 nm) sections were prepared and stained with 1% toluidine blue. Ultrathin (60–70 nm) sections were cut using an ultramicrotome (Ultracut-N; Reichert-Jung), contrasted with uranyl acetate and lead citrate, examined using a JEM-1010 electron microscope (Jeol) and photographed. At least 20 photomicrographs were analyzed for each mouse to quantify the postsynaptic density (PSD) length, spine number and the percentage of perforated spines.

DiI staining. Lipophilic dye 1,1′-(dioctadecyl-3,3,3′,3′-tetramethylindocarbocyanine perchlorate (DiI) (Invitrogen) staining was performed as described previously (Satoh et al., 2007).

Immunohistochemistry. Immunohistochemical studies were performed as previously described (Satoh et al., 2011). Briefly, paraffin sections (5 μm thick) were deparaffinized and immersed in unmasking solution (Vector H3300; Vector Laboratories) for antigenic retrieval and heated in an autoclave (121°C) for 5 min. Then, sections were incubated with a nonspecific blocking reagent (Dako) for 1 h to reduce background staining.

For bright-field dye staining (Fig. 1*G*), sections were then incubated with a primary antibody (anti-ERK2; mouse monoclonal, 1:1000; BD Transduction Laboratories) overnight in a humidified chamber at 4°C, followed by application of a biotinylated horse anti-mouse IgG secondary antibody (Vector Laboratories). For signal amplification, sections were incubated with an avidin-biotin-horseradish peroxidase complex (ABC Elite kit; Vector Laboratories) and visualized by a 3,3′-diaminobenzidine tetrachloride (Vector Laboratories) reaction according to the manufacturer's instructions. Finally, the sections were counterstained with hematoxylin. PBS was used for rinses.

For fluorescent staining, the primary antibodies used were anti-ERK2 (Fig. 2; rabbit polyclonal, 1:400; Cell Signaling Technology), anti-glial fibrillary acidic protein (GFAP) (see Fig. 4; mouse monoclonal, 1:50; Sigma), or anti-NeuN (Fig. 3; mouse monoclonal, 1:100; Millipore). After application of primary antibody overnight in a humidified chamber at 4°C, sections were incubated with secondary antibodies. The secondary antibodies used were Alexa-Fluor 488-conjugated goat anti-mouse IgG (1:400; Invitrogen) or Cy3-conjugated goat anti-mouse IgG (1:400; Jackson Immunoresearch) for primary antibodies derived from mouse. For primary antibody derived from rabbit, Cy3-conjugated goat anti-rabbit IgG antibody (1:400; Jackson Immunoresearch) was used. Sections were examined with a wide-field or confocal fluorescence microscopy using Nikon C1 system (Nikon). Samples from at least four mice per genotype were examined in each experiment.

Cell counting. Cell number was assessed using the StereoInvestigator system (MicroBrightField). The boundaries were drawn using StereoInvestigator and stained cells were counted within sampling frames chosen in a systematically random manner within the areas of interest. The number of cortical cells stained for NeuN was counted in the dorsolateral portion of the cerebral cortex, from the retrosplenial cortex medially up to the rhinal fissure ventrolaterally.

Western blot analysis. Preparation of protein extracts was performed as previously described (Satoh et al., 2007). Briefly, the amount of protein in each sample was measured using a BCA assay kit (Pierce). Samples were subjected to SDS-PAGE. The proteins were transferred onto an Immobilon-P membrane (Millipore). The blots were then immunoreacted with primary antibodies. The primary antibodies used were anti-ERK1/2 (rabbit polyclonal, 1:1000; Cell Signaling Technology), anti-phospho-ERK1/2 (rabbit polyclonal, 1:1000; Cell Signaling Technology), or anti-β-actin (mouse monoclonal, 1:2500; Sigma). Then, the primary antibodies were recognized using horseradish peroxidase (HRP)-conjugated secondary antibodies. Detection was performed with chemiluminescent substrates for HRP (Super Signal West Pico; Pierce or ECL plus; GE Healthcare). The signals were analyzed using an LAS3000 digital imaging system (Fujifilm). Samples from at least five mice per genotype were examined in each experiment.

Behavioral tests. Mice used for behavioral tests were age-matched male littermates except for the maternal behavior test and pup exchange test. For the maternal behavior and pup exchange test, age-matched female littermates were used. Since the *Erk2* CKO mother does not care well for their pups, all mice used in the behavioral tests were borne and reared by control mothers, except for those used in the pup exchange test. The apparatuses used in this study were made by O'Hara & Co., Ltd. except where described.

Open field test. The open field test was performed as described previously (Satoh et al., 2007). Briefly, activity was measured as the total distance traveled (meters) in 10 min in the open field chamber (50 cm long × 50 cm wide × 40 cm high). The center square of the open field, comprising 50% of the total area, was defined as the "central area" of the open field. Mice used for the test were 9–11 weeks old.

Elevated plus-maze test. The elevated plus-maze (EPM) test was performed as described previously (Satoh et al., 2007). Briefly, mouse behavior was recorded during a 10 min test period. The percentage of time spent in the open arms was used as an index of anxiety-like behavior.

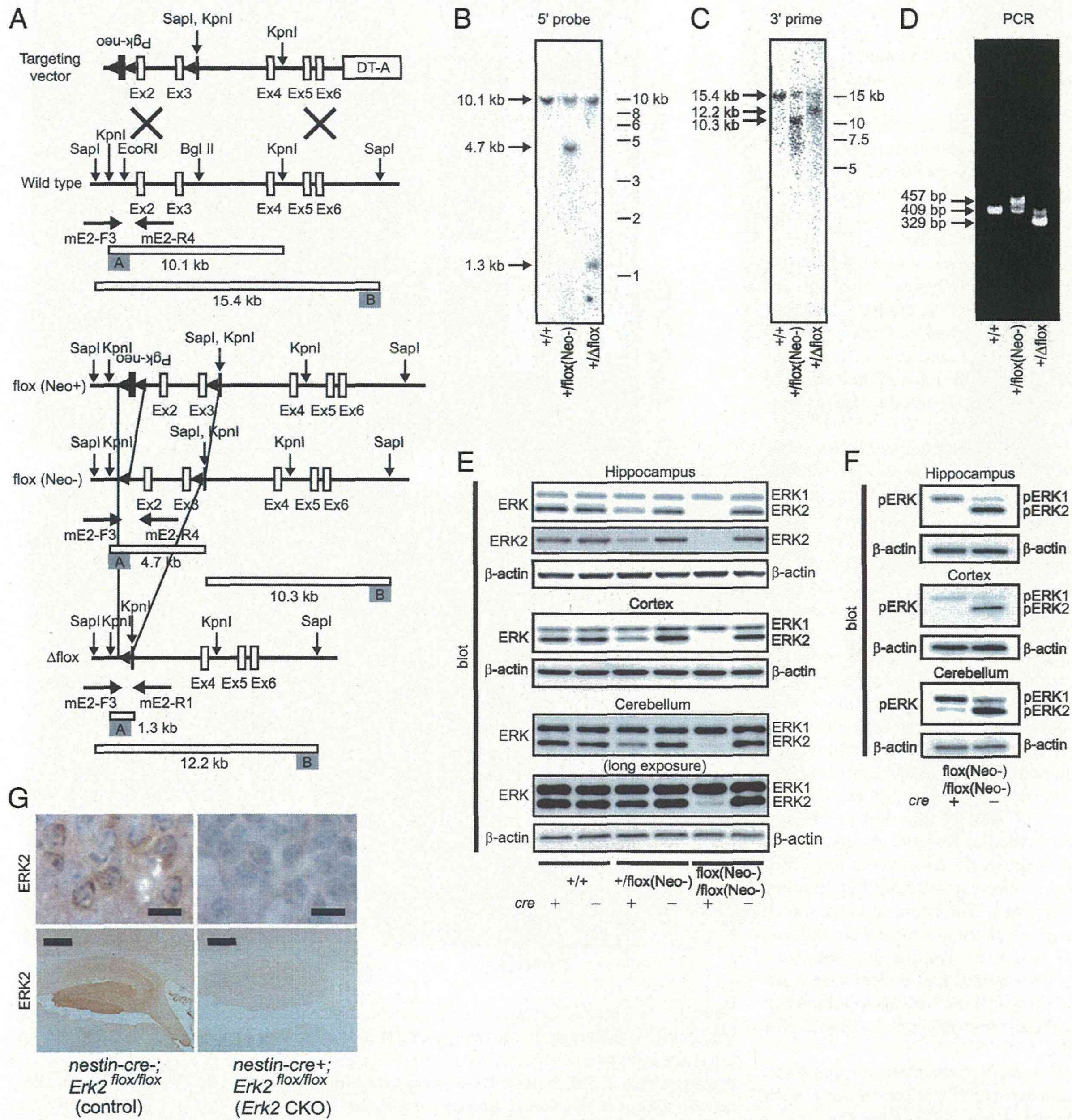

Figure 1. Generation of *Erk2* CKO mice. ***A***, Schematic diagram of targeted knock-out of the mouse *Erk2* gene. The *Erk2*(*flox(Neo*+)) allele is converted to the *Erk2*(*flox(Neo*−)) allele by *in vivo cre*-mediated partial recombination using EIIA-*cre* mice. White boxes represent *Erk2* exons and black boxes represent the *Pgk-neo* cassette. The 5′ and 3′ outer probes used for Southern blotting are shown as gray boxes. The locations of the primers used for genotyping are indicated underneath each scheme. ***B***, ***C***, Southern blot analysis of wild-type and mutant mouse genomic DNA. DNA samples are digested with KpnI and hybridized with the 5′ (***B***) or 3′ (***C***) outer probe. The positions and sizes of the wild-type and mutant fragments are indicated. ***D***, PCR genotyping of wild-type and mutant mice. The positions and sizes of PCR fragments for wild-type and mutant mice are indicated. ***E–G***, Expression profile in adult *Erk2* CKO mice. ***E***, Expression of ERK1 and 2 in extracts of the hippocampus, cortex and cerebellum. ***F***, Phosphorylation status of ERK1 and 2 in basal conditions. In ***E*** and ***F***, β-actin serves as the control for protein loading. ***G***, Loss of ERK2 protein in the nervous system in *Erk2* CKO mice. Immunohistochemical analysis of the hippocampus (bottom) and hippocampal pyramidal cells (top) show the distribution of ERK2 in neuronal cells from *nestin-cre*−; *Erk2* $^{flox/flox}$ (control) mice, and that ERK2 is absent in *nestin-cre*+; *Erk2* $^{flox/flox}$ (*Erk2* CKO) mice. Slides are counterstained with hematoxylin. Scale bars: top, 10 μm; bottom, 500 μm.

Mice used for the test were 9–11 weeks old (the same set of mice as in the open field test).

Maternal behavior test. The maternal behavior test was conducted as described previously (Jin et al., 2007). Briefly, pregnant females were individually housed for a few days before parturition and examined for maternal behavior on the morning of parturition. After a 10 min separation of the mother from her pups, the dam was put in one corner of a cage and three of her pups were placed in different corners of the same cage. Then, she was observed for 20 min with minimal disturbance, and the time spent in crouching over the three pups was recorded. The percentage of newborns scattered was recorded at the end of the test. Mice used for the test were 13–15 weeks old.

Pup exchange test. The pup exchange test was conducted using six *Erk2* CKO and control mother couples. Pups that were born on the same day were exchanged during the first day after birth. The number of surviving pups was followed until weaning. Mice used for the test were 11–15 weeks old.

Resident-intruder test. The resident-intruder test was performed as previously described (Takayanagi et al., 2005). Twenty-week-old resident males were individually housed for 2 weeks before testing. Eight-

week-old wild-type mice, housed in groups, were used as intruders. New intruder mice were used in each test. The attack duration, frequency and latency to first attack were recorded for 10 min.

Social recognition test. The social recognition test was conducted as described previously (Satomoto et al., 2009). We transferred 16-week-old mice from group to individual housing for 7 d before testing to permit establishment of a home-cage territory. Testing began when an ovariectomized female mouse was introduced into the home cage of each male mouse for a 1 min confrontation. At the end of the 1 min trial, the stimulus animal was removed and returned to an individual cage. This sequence was repeated for four trials with 10 min intertrial intervals, and each stimulus mouse was introduced to the same male resident in all four trials. In a fifth trial, another ovariectomized stimulus female was introduced to a resident male mouse. The stimulus females were all wild-type mice. Investigation was defined as direct, active and olfactory exploration of the female by the subject male mice. In general, this consisted of nosing and sniffing of the perioral and anogenital regions, as well as close following and pursuit. Aggressive posturing and sexual behaviors including mounting were not included in the measures of investigation. Females were exposed to only one male per day to reduce male odor contamination.

Sociability test in the open field chamber. The preference for interaction with animate (caged adult mouse) versus inanimate (caged dummy mouse) targets (sociability) was examined in the open field chamber according to a slightly modified method of Kwon et al. (2006). Animate or inanimate targets were put into cylindrical cages allowing olfactory but minimal tactile interaction. The cylindrical cage was 10 cm in height, with a diameter of 9 cm and bars spaced 7 mm apart. Sniffing directed at the cage was scored for 10 min under 70 lux lighting conditions. We used 16-week-old mice in this test and all animate targets were wild-type male mice.

Sociability and social novelty test in a three-room chamber. Social preference for novelty was performed in a three-room chamber as previously described (Moy et al., 2004). Each chamber was 20 cm long × 40.5 cm wide × 30 cm high. Dividing walls were made from clear Plexiglas, with small openings allowing access into each chamber. In the test, mice were initially allowed to explore the chambers for 10 min. After the habituation period, a caged wild-type male mouse, which had no prior contact with the subject mice, was placed in one of the side chambers. The cylindrical cages used were the same as those used in the sociability test in the open field. The subject mouse was placed in the middle chamber, and then the mouse was allowed to interact with an empty cage in one room versus a caged social target in another room for 10 min (sociability test). At the end of the first 10 min session, each mouse was tested in a second 10 min session to quantify social preference for a new stranger (social novelty test). The unfamiliar new stranger mouse was placed in an identical cage in the chamber that had been empty during the first 10 min session. The test mouse had a choice between the first, already-investigated mouse (familiar) and the novel unfamiliar mouse (novel). The time spent in each chamber was measured. Ten-week-old mice were used for the study.

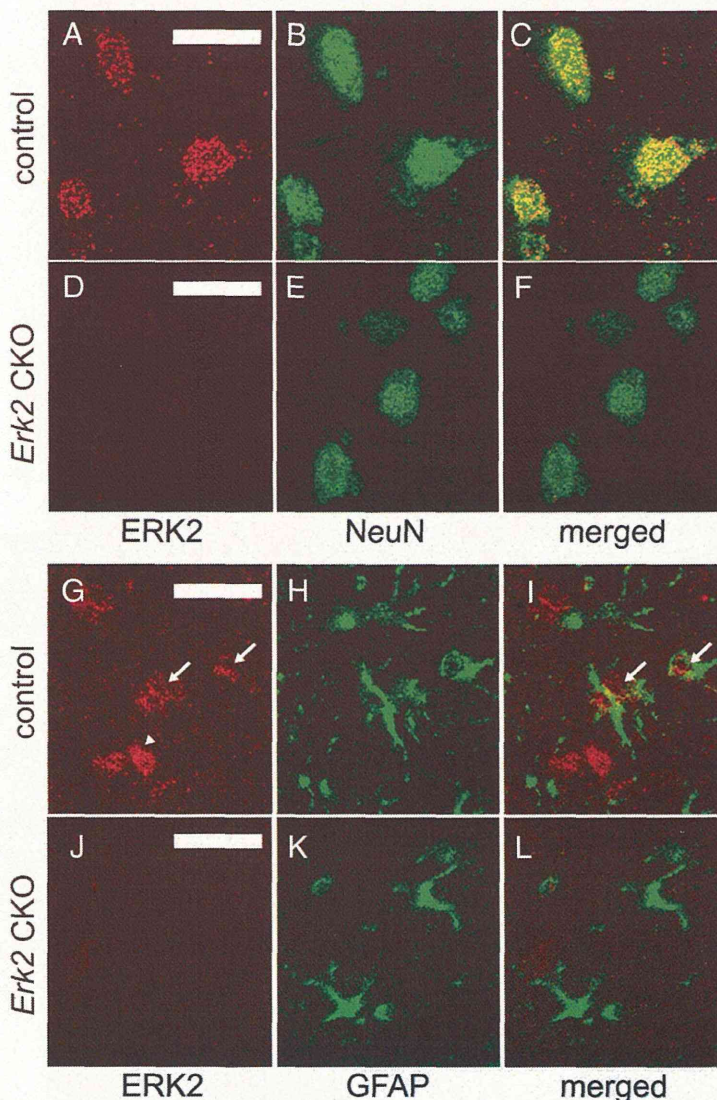

Figure 2. ERK2 protein is abrogated in neuronal and glial cells in *Erk2* CKO mice. ***A–C***, ERK2 is expressed in neuronal cells in control mice at 12 weeks of age. Double staining for ERK2 (***A***) and the postmitotic neuronal marker NeuN (***B***) in the neocortex show that ERK2 is expressed in neurons, as indicated by colocalization (***C***). ***D–F***, ERK2 is abrogated in neuronal cells in *Erk2* CKO mice. Double staining for ERK2 (***D***) and NeuN (***E***) with a merged image (***F***) show that ERK2 is not detectable in neuronal cells in *Erk2* CKO mice. ***G–I***, ERK2 is expressed weakly in astrocytes in control mice. Double staining for ERK2 (***G***) and the astrocyte marker GFAP (***H***) in the neocortex with a merged image (***I***) show partial colocalization of ERK2 and GFAP, indicating that ERK2 is expressed weakly in some astrocytes (arrows) although not in other astrocytes. Arrowhead indicates probable expression of ERK2 in neurons. ***J–L***, ERK2 is abrogated in astrocytes in *Erk2* CKO mice. Double staining for ERK2 (***J***) and GFAP (***K***) with a merged image (***L***) show that ERK2 is not detectable in astrocytes in *Erk2* CKO mice. Scale bars, 20 μm.

Olfactory test. The olfactory test was conducted as described previously (Satomoto et al., 2009). Briefly, mice were habituated to the flavor of a novel food (blueberry cheese) for 3 d before testing. On the fourth day, following 24 h food deprivation, a piece of blueberry cheese was buried under 2 cm of bedding in a clean cage. The mice were placed in the cage, and the time required to find the food was measured. The same set of mice was used as in the sociability and social novelty test in the three-room chamber.

Novelty test. The novelty test was performed as previously described (Satomoto et al., 2009). Mice were housed individually and activity was measured as the total time spent interacting with an inanimate novel object (a small red tube) in 10 min. The same set of mice was used as in the sociability and social novelty test in the three-room chamber.

Nest formation test. Nest formation was examined as described previously (Lijam et al., 1997) with minor modification. Six cages of male controls and six of male *Erk2* CKO mice ($n = 4$ mice per cage) were used